
Article:
Onel, L, Blitz, MA, Seakins, PW et al. (2020) Kinetics of the Gas Phase Reactions of the Criegee Intermediate CH2OO with O3 and IO. The Journal of Physical Chemistry A. acs.jpca.0c04422. ISSN: 1089-5639

https://doi.org/10.1021/acs.jpca.0c04422

Kinetics of the Gas Phase Reactions of the Criegee Intermediate CH_2OO with O_3 and IO

Lavinia Onel,[1] Mark Blitz,[1,2] Paul Seakins,[1] Dwayne Heard,[1] and Daniel Stone[1*]

[1] School of Chemistry, University of Leeds, Leeds, LS2 9JT, UK

[2] National Centre for Atmospheric Science, University of Leeds, Leeds, LS2 9JT, UK

* Corresponding Author: d.stone@leeds.ac.uk, +44 113 343 6508

Abstract

The kinetics of the gas phase reactions of the Criegee intermediate CH_2OO with O_3 and IO have been studied at 296 K and 300 Torr through simultaneous measurements of CH_2OO, the CH_2OO precursor (CH_2I_2), O_3, and IO using flash photolysis of $CH_2I_2/O_2/O_3/N_2$ mixtures at 248 nm coupled to time-resolved broadband UV absorption spectroscopy. Experiments were performed under pseudo-first-order conditions with respect to O_3, with the rate coefficients for reactions of CH_2OO with O_3 and IO obtained by fitting to the observed decays of CH_2OO using a model constrained to the measured concentrations of IO. Fits were performed globally, with the ratio between the initial concentration of O_3 and the average concentration of IO varied in the range 30 to 700, and gave $k_{CH2OO+O3} = (3.6 \pm 0.8) \times 10^{-13}$ cm^3 molecule^{-1} s^{-1} and $k_{CH2OO+IO} = (7.6 \pm 1.4) \times 10^{-11}$ cm^3 molecule^{-1} s^{-1} (where the errors are at the 2σ level). The magnitude of $k_{CH2OO+O3}$ has a significant effect on the steady state concentration of CH_2OO in chamber studies. Atmospheric implications of the results are discussed.

KEYWORDS *Criegee intermediate, CH_2OO, ozone, IO, kinetics, laser flash photolysis, time-resolved, broadband UV absorption spectroscopy*

Introduction

A significant fraction of unsaturated volatile organic compounds (VOCs) in the atmosphere are oxidised by ozone in ozonolysis reactions which result in the production of highly reactive Criegee intermediates (CIs) such as CH_2OO.[1, 2] For isoprene, the most abundant non-methane VOC in the atmosphere, ozonolysis represents ~10% of the total global sink, and it is a greater sink for

monoterpenes and sesquiterpenes, which react more rapidly with O_3.[3] In urban environments, the oxidation of unsaturated VOCs initiated by ozone has been demonstrated to be a significant source of OH radicals in low light conditions in winter and at nighttime.[4, 5]

The nascent CI generated in an ozonolysis reaction is vibrationally excited and may either decompose or lose its excess internal energy through collisions with surrounding gas phase molecules, leading to the production of a stabilised CI (SCI).[2] The chemistry of SCIs can impact atmospheric composition, and thus air quality and climate, through reactions with water,[6] water dimers,[7, 8] SO_2,[9-12] and NO_2,[9, 10, 13] among other species. In chamber experiments to investigate atmospherically important ozonolysis reactions, the behaviour of SCIs can influence measurements of other reactants and products used to probe reaction mechanisms, with the experimental conditions required for such studies potentially promoting reactions which may not be representative of atmospheric conditions but are important in the overall analysis of the experimental data. The self-reaction of the CH_2OO Criegee intermediate, for example, has a minor role in the atmosphere, but consideration of its impact on laboratory studies of other atmospherically important reactions can be critical to accurate measurements.[14] Ozonolysis experiments in atmospheric simulation chambers, in which the chemistry of SCIs is typically inferred from measurements of other species, are often performed at relatively high alkene and O_3 concentrations, and there is thus the potential for reactions of alkenes and O_3 with any SCIs produced in the system.

The kinetics of SCI reactions with alkenes have been investigated in a number of studies,[15-17] enabling quantification of the role of such reactions in ozonolysis experiments. In contrast, the potential for reactions of SCIs with O_3 have received relatively little attention. There has been a single experimental study[18] of the reaction between the simplest SCI, CH_2OO, with O_3 (R1), giving a rate coefficient of $(6.7 \pm 0.5) \times 10^{-14}$ cm^3 molecule^{-1} s^{-1} between 30 and 100 Torr at 298 K, with theoretical studies indicating production of HCHO + 2 O_2.[17, 19-22]

$$CH_2OO + O_3 \rightarrow HCHO + 2\ O_2 \qquad \text{(R1)}$$

However, the theoretical studies do not agree on the mechanism for R1, and there are significant discrepancies in the predicted kinetics. Kjaergaard *et al*.[19] and Wei *et al*.[20] predicted the direct formation of a cycloaddition intermediate between CH_2OO and O_3, with Kjaergaard *et al*. predicting the formation of a second intermediate prior to production of the final HCHO + 2 O_2 products but Wei *et al*. indicate a direct link between the cycloaddition intermediate and final products. Challenges associated with determination of the energy of the transition state between the reactants and the cycloaddition intermediate led Kjaergaard *et al*. to recommend a lower limit of 10^-

[18] cm^3 $molecule^{-1}$ s^{-1} for $k_{CH2OO+O3}$ at 1 atm and 298 K, while Wei *et al.*[20] indicated a barrier of 14.1 kcal mol^{-1} which suggests a rate coefficient < 10^{-20} cm^3 $molecule^{-1}$ s^{-1} under such conditions.[22]

Subsequent theoretical studies reported by Vereecken *et al.*[17, 22] demonstrated the existence of a chain addition pathway occurring via the barrierless formation of a pre-reactive complex owing to electrostatic interactions between CH_2OO and O_3, with the reaction proceeding through a submerged transition state. No evidence was found for the cycloaddition pathway, and it was noted that, even if possible, it would be both energetically and entropically unfavourable. Initially, it was predicted that $k_{CH2OO+O3} = 1 \times 10^{-12}$ cm^3 $molecule^{-1}$ s^{-1} at 298 K,[17] with subsequent calculations at higher levels of theory leading to a revised value of $k_{CH2OO+O3} = 4 \times 10^{-13}$ cm^3 $molecule^{-1}$ s^{-1}, but with an estimated uncertainty of at least one order of magnitude.[22] Maranzana and Tonachini[21] discussed the challenges associated with accurate calculation of the potential energy surface for the reaction in detail, and reported high level calculations that support the conclusion of Vereecken *et al.*[22] regarding the lack of evidence for the cycloaddition pathway. While no kinetics were evaluated by Maranzana and Tonachini, the calculations presented suggest a barrier to reaction, implying a slower reaction than predicted by Vereecken *et al.*[22] However, the results also indicated the importance of dynamical correlations that affect both quantitative and qualitative assessment of the reaction,[21] highlighting the need for direct kinetic measurements.

Thus far, there has been a single experimental study of the reaction between CH_2OO and O_3 (R1), in which CH_2OO was generated by the laser flash photolysis of CH_2I_2 in the presence of O_2 at a wavelength of 352 nm (R2 and R3):[18]

$$CH_2I_2 + h\nu \rightarrow CH_2I + I \qquad \text{(R2)}$$

$$CH_2I + O_2 \rightarrow CH_2OO + I \qquad \text{(R3a)}$$

$$CH_2I + O_2 + M \rightarrow CH_2IO_2 + M \qquad \text{(R3b)}$$

Kinetics were determined under pseudo-first-order conditions with respect to O_3 using infrared quantum cascade laser spectroscopy to monitor the integrated absorption intensity of the CH_2OO ν_4 band in the region 1285.7–1285.74 cm^{-1}. The rate coefficient obtained at 298 K, $k_{CH2OO+O3} = (6.7 \pm 0.5) \times 10^{-14}$ cm^3 $molecule^{-1}$ s^{-1}, was found to be independent of pressure from 30 to 100 Torr. No other species involved in the reaction system such as the IO radical, formed mainly by the reaction of I atoms, produced in (R2) and (R3a), with O_3 (R4), were monitored.

$$I + O_3 \rightarrow IO + O_2 \qquad \text{(R4)}$$

However, the experimental observations of CH_2OO combined with numerical simulations suggested a rapid reaction between CH_2OO and IO (R5) occurring in competition with the reaction of CH_2OO with O_3 (R1), with the rate coefficient $k_{CH2OO+IO}$ estimated to be 1.5×10^{-10} cm^3 $molecule^{-1}$ s^{-1}.

$$CH_2OO + IO \rightarrow \text{Products} \qquad \text{(R5)}$$

In this work we report a study of the kinetics of $CH_2OO + O_3$ and CH_2OO + IO at 296 K and 300 Torr using flash photolysis of $CH_2I_2/O_2/O_3/N_2$ mixtures at 248 nm coupled to time-resolved broadband UV absorption spectroscopy. This technique enables the determination of kinetic parameters for complex chemical systems involving several species with overlapping absorption spectra,[23] and can be used to provide simultaneous measurements of changes in concentrations of CH_2I_2, CH_2OO, IO and O_3.

Experimental

The kinetics of the $CH_2OO + O_3$ and CH_2OO + IO reactions were studied using laser flash photolysis of $CH_2I_2/O_2/N_2$ (O_2:N_2 = 98:2) gas mixtures, coupled with broadband time-resolved UV absorption spectroscopy. The experimental apparatus has been described in detail previously[24] and has been used to determine the absorption cross-sections for CH_2OO[14] and the kinetics of CH_2OO reactions.[7, 11, 14]

Precursor gases were mixed in a gas manifold and flowed into the reaction cell at known flow rates determined by calibrated mass flow controllers. CH_2I_2 was introduced into the gas manifold by passing a known flow of N_2 through a bubbler containing liquid CH_2I_2 held at a constant temperature in an ice bath. The reaction cell was a 150 cm long glass tube of 5 cm inner diameter sealed with fused silica windows at both ends. The total flow rate was 30 standard litres per minute (slm), corresponding to a residence time in the cell of ~6 s under standard conditions. The total pressure in the cell was maintained at 300 Torr and measured by a capacitance manometer (MKS Instruments). Experiments were carried out at 296 K in O_2 (BOC, 99.5 %) using CH_2I_2 as supplied (Alfa Aesar 99%) and O_3 produced by an ozone generator (Fischer technology OZ500).

Chemistry within the reaction cell, shown in Table 1, was initiated by an excimer laser (KrF, Lambda-Physik CompEx 210) operating at a wavelength of 248 nm with a typical laser fluence of $0.6–1.0 \times 10^{17}$ photon cm^{-2}. A wavelength of 248 nm was used in preference to 351 or 355 nm as it was necessary to use a cut-on filter to minimise the impact of scattered photolysis light and, at 351

or 355 nm, this would remove a region of the spectrum with significant CH_2OO absorption. The photolysis light was aligned along the length of the reaction cell with a pulse repetition rate of 0.15 Hz, ensuring a fresh gas mixture in the cell for each laser pulse. The photolysis of O_3 at 248 nm generated $O(^1D)$ and $O(^3P)$ in a ratio of 9:1 (R6).[25] The measurements therefore used gas mixtures containing 98% O_2 (~9.5×10^{18} molecule cm^{-3}) to ensure rapid regeneration of O_3. Numerical simulations (described in the Supporting Information) show that O_3 was regenerated on a timescale of ~100 μs following photolysis owing to reactions R7 and R8.

$$O_3 + h\nu\ (248\ nm) \rightarrow 0.9\ O(^1D) + 0.1\ O(^3P) + O_2 \qquad (R6)$$

$$O(^1D) + M\ (98\%\ O_2,\ 2\%\ N_2) \rightarrow O(^3P) + M \qquad (R7)$$

$$O(^3P) + O_2 + M \rightarrow O_3 + M \qquad (R8)$$

Concentrations of CH_2I_2 and O_3 were chosen to ensure pseudo-first-order conditions for the reaction between CH_2OO and O_3 and to provide a range of $[O_3]$:[IO] ratios, whilst also avoiding aerosol formation observed at higher $[CH_2I_2]$ and $[O_3]$ over the timescales of the kinetic measurements (further details are given in the Supporting Information). The initial concentrations of CH_2I_2 and O_3 were determined from averages of the CH_2I_2 and O_3 UV absorption spectra measured in the cell before and after each kinetic run. Details of the procedures for determination of the initial concentrations of CH_2I_2 and O_3, and of the experimental conditions, are provided in the Supporting Information.

The total UV–visible absorption was monitored using a laser-driven light source (LDLS, Energetiq EQ-99X), which provides ~10 mW cm^{-2} of light at wavelengths between 200 nm and 800 nm. The probe light was aligned in a seven pass arrangement described previously,[24] resulting in a total effective pathlength of (443 ± 21) cm (see Supporting Information).

The output beam was passed through a sharp cut-on filter (248 nm RazorEdge ultrasteep long-pass edge filter, Semrock) to minimise the impacts of scattered excimer light and focused onto a fibre optic via a fibre launcher (Elliot Scientific). The output from the fibre optic was directed through a 25 μm slit onto a spectrograph equipped with a diffraction grating of 300 grooves/mm and imaged onto an integrated thermoelectrically cooled charge-coupled device (CCD) detector with a spectral resolution (FWHM) of 1 nm (FER-SCI-1024BRX, Princeton Instruments). The spectral and temporal information were mapped spatially along the horizontal and vertical directions of the CCD, respectively. The sensor format was 1024 × 512 (width × height) pixels with an illuminated region of interest of 1024 × 10 pixels and a storage region of 1024 × 265 pixels. The rows of the illuminated region were exposed to the incident light simultaneously (exposure time = 10 – 100 μs)

and then shifted one-by-one vertically (on the time axis) from the illuminated region to the storage region with a programmable frame rate from 5.6 μs/row to 35 μs/row. The resulting overall time resolution was thus on the order of hundreds of μs. The instrument response function resulting from the rapid shift of photocharge on the CCD used to provide temporal information is described in the Supporting Information.

Wavelength calibration was performed by measuring the well-known Hg emission spectrum from a low pressure Hg pen-ray lamp (Oriel). Timing of the excimer laser and camera was controlled by a delay generator (SRS DG535). Intensity data were typically averaged for 400 photolysis shots and transferred to a PC for analysis.

Results

The observed total UV absorption recorded as a function of wavelength (λ) and time (t), $A(\text{tot})_{\lambda,t}$, was analysed between 300–450 nm to determine the changes to concentrations of CH_2OO, IO and CH_2I_2 as a function of time following photolysis by fitting the reference absorption cross-sections for CH_2OO,[14] IO[26] and CH_2I_2[25] to $A(\text{tot})_{\lambda,t}$ at each time point (equation E1).

$$A(\text{tot})_{\lambda,t} = \ln\left(\frac{I_{\lambda,0}}{I_{\lambda,t}}\right) = \sum_i \sigma_{i,\lambda} \,.\, [i]_t \,.\, l \qquad \text{(E1)}$$

where $I_{\lambda,0}$ is the average pre-photolysis intensity at wavelength λ, $I_{\lambda,t}$ is the post-photolysis intensity at wavelength λ and time t, $\sigma_{i,\lambda}$ is the cross section of species i at wavelength λ, $[i]_t$ is the concentration of species i at time t, and l is the total pathlength (443 ± 21) cm. Figure 1 shows a typical fit to the observed absorbance following photolysis.

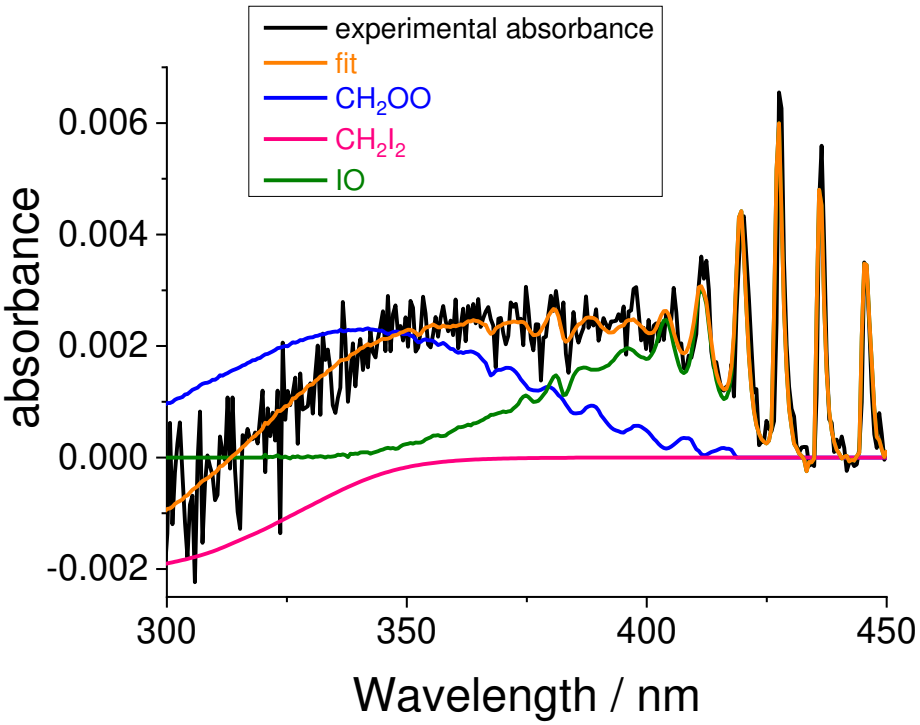

Figure 1: Observed absorbance (black), total fit (orange), and the individual contributions from CH_2OO (blue), IO (green) and CH_2I_2 (pink) determined by fitting reference spectra to the measured absorbance using equation E1 at t = 0.3 ms following photolysis. For these data the exposure time of the CCD detector to the incident light was 50 μs, T = 296 K, p = 300 Torr, with initial reagent concentrations $[CH_2I_2] = 1.2 \times 10^{13}$ molecule cm^{-3} and $[O_3] = 1.1 \times 10^{14}$ molecule cm^{-3}. The concentrations of the species contributing to the total absorbance were: $[CH_2OO] = 3.7 \times 10^{11}$ molecule cm^{-3}, $[IO] = 6.5 \times 10^{11}$ molecule cm^{-3} and $\Delta[CH_2I_2] = -1.1 \times 10^{12}$ molecule cm^{-3}.

Contributions from ozone absorbance in the range 300 to 450 nm used to determine concentration-time profiles from fits to equation E1 were negligible for the concentrations of ozone used to determine kinetics, and fit results for CH_2OO, IO, and CH_2I_2 were insensitive to the inclusion of ozone in the fits (see Supporting Information for further details). However, fits at wavelengths between 285 and 450 nm were also performed for experiments with higher concentrations of O_3 (> 1×10^{14} molecule cm^{-3}) to confirm the rapid regeneration of O_3 following photolysis. The observed depletion in O_3 concentration returned to the baseline (< 5.0×10^{10} molecule cm^{-3}) rapidly (<0.1 ms) following photolysis (see Supporting Information for further details), and the ozone concentration remained effectively constant during the decay of CH_2OO (20-100 ms) to give pseudo-first-order conditions with respect to O_3.

Figure 2 shows typical concentration-time profiles for CH_2OO and IO. For all experiments, the production of CH_2OO from $CH_2I + O_2$ was rapid, occurring with a pseudo-first-order rate coefficient > 10^7 s^{-1}. However, the observed concentration-time profiles are given by a convolution of the 'true' behaviour with an instrument response function (IRF), which, for CH_2OO, resulted in an initial increase in the observed concentration prior to the subsequent decay. The initial growth

was rapid, occurring within hundreds of μs, in comparison to the timescale for CH_2OO decay, which typically occurred on a timescale of tens of ms, and the IRF could thus be excluded from analysis of CH_2OO kinetics. Further details regarding the IRF are given in the Supporting Information.

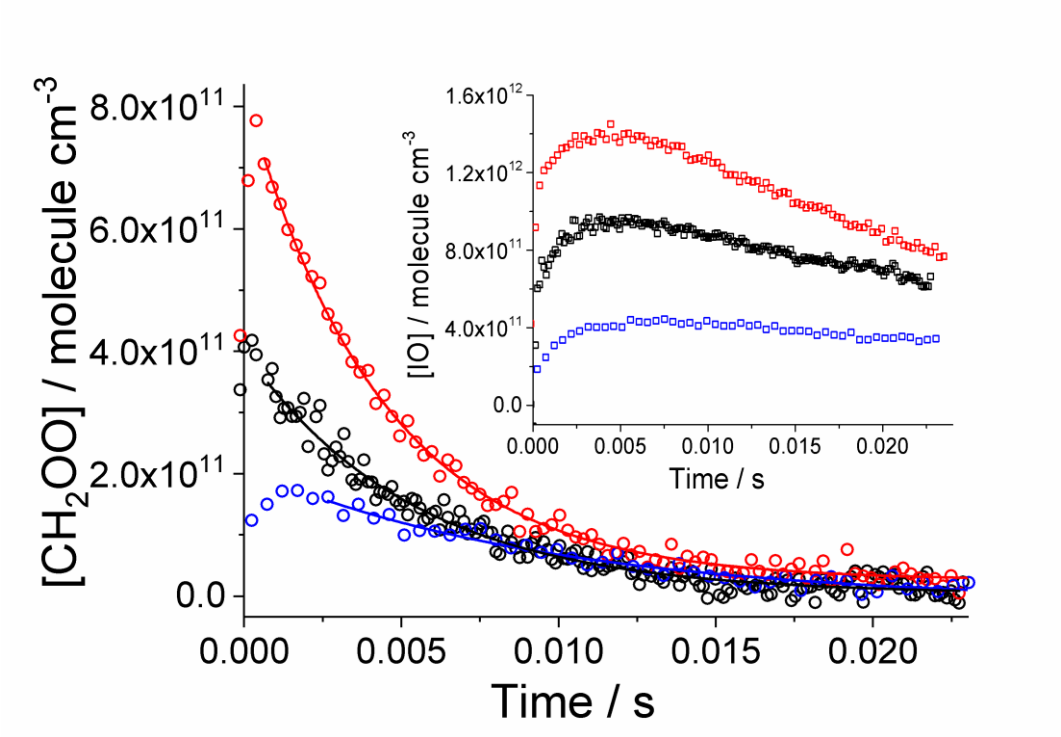

Figure 2: Examples of observations of CH_2OO (open circles) and fit results (solid lines) obtained by numerical integration of all traces simultaneously. Red circles: $[O_3] = 1.3 \times 10^{14}$ molecule cm^{-3} and $[CH_2I_2] = 1.6 \times 10^{13}$ molecule cm^{-3}; black circles: $[O_3] = 2.2 \times 10^{14}$ molecule cm^{-3} and $[CH_2I_2] = 6.3 \times 10^{12}$ molecule cm^{-3}; blue circles: $[O_3] = 2.1 \times 10^{14}$ molecule cm^{-3} and $[CH_2I_2] = 3.5 \times 10^{12}$ molecule cm^{-3}. For all experiments, the production of CH_2OO from $CH_2I + O_2$ occurred with a pseudo-first-order rate coefficient greater than 10^7 s^{-1}. During the fit [IO] is constrained to the experimental data shown in the inset. For all data, $T = 296$ K and $p = 300$ Torr.

Kinetics for $CH_2OO + O_3$ and CH_2OO + IO were obtained by fitting to the experimental data using numerical integration of the chemistry scheme shown in Table 1 in a MATLAB model using a Levenberg-Marquardt algorithm. Fits to a number of temporal decays for CH_2OO were performed simultaneously, with the rate coefficients describing the chemistry treated as global parameters. Owing to the significant uncertainties related to the formation of IO following photolysis of $CH_2I_2/O_2/N_2$,[14,27, 28,29] the model was constrained to the measured concentrations of IO. Further details of the uncertainties surrounding the temporal behaviour of IO during the kinetic experiments are given in the Supporting Information. In order to maximise the sensitivity to both $k_{CH2OO+O3}$ and $k_{CH2OO+IO}$, the ratio between the initial O_3 concentration and the average IO concentration during the CH_2OO decay was varied in the range from 30 to 700 through use of a range of O_3 and IO concentrations ((0.1–5.0) × 10^{14} molecule cm^{-3} and (0.2–2.0) × 10^{12} molecule cm^{-3}, respectively),

and measurements made in the absence of O_3 were also included in the analysis (experimental conditions provided in the Supporting Information). All the fit results are shown in the Supporting Information. Figure 2 shows examples of results obtained for a range of O_3 and IO concentrations.

Reaction	Rate coefficient / cm^3 $molecule^{-1}$ s^{-1} or s^{-1}	Reference
$CH_2OO + I \rightarrow$ Products	$(1.5 \pm 0.5) \times 10^{-11}$	This work[a]
$CH_2OO + CH_2OO \rightarrow$ Products	$(8.0 \pm 1.1) \times 10^{-11}$	Mir *et al.*[14]
$CH_2OO + O_3 \rightarrow$ Products	$(3.6 \pm 0.8) \times 10^{-13}$	This work[a]
$CH_2OO + IO \rightarrow$ Products	$(7.6 \pm 1.4) \times 10^{-11}$	This work[a]
$CH_2IO_2 + CH_2IO_2 \rightarrow 2\ CH_2IO + O_2$	9.0×10^{-11}	Gravestock *et al.*[29]
$CH_2IO_2 + I \rightarrow CH_2IO + IO$[b]	3.5×10^{-11}	Gravestock *et al.*[29]
$CH_2IO \rightarrow CH_2O + I$	1.0×10^{5}	Gravestock *et al.*[29]
$I + O_3 \rightarrow$ Products	1.28×10^{-12}	Tucceri *et al.*[30]
$I + I \rightarrow I_2$	1.83×10^{-13}	Jenkin *et al.*[31]

Table 1: Chemistry scheme used in numerical simulations. [a] Determined by the fit to the experimental temporal decays of CH_2OO with the model constrained to the measured concentrations of IO (see main text). Errors are quoted at the 2σ level. [b] IO is shown to balance the reaction. The model was not use to simulate [IO] vs. time as [IO] was fixed to the experimental value at each time point (main text).

The fit results gave $k_{CH2OO+O3} = (3.6 \pm 0.8) \times 10^{-13}$ cm^3 $molecule^{-1}$ s^{-1} and $k_{CH2OO+IO} = (7.6 \pm 1.4) \times 10^{-11}$ cm^3 $molecule^{-1}$ s^{-1} (errors are quoted at the 2σ level), and returned a value of $k_{CH2OO+I} = (1.5 \pm 0.5) \times 10^{-11}$ cm^3 $molecule^{-1}$ s^{-1}, although results for $k_{CH2OO+O3}$ and $k_{CH2OO+IO}$ were not sensitive to the value for $k_{CH2OO+I}$ owing to low I atom concentrations as a result of efficient titration of I to IO in R4. Mir *et al.*[14] found that the reaction $CH_2OO + I$ can be treated as a loss process for CH_2OO and I with unspecified products in model fits to decays of CH_2OO produced in the $CH_2I_2/O_2/N_2$ photolytic system. The value obtained for $k_{CH2OO+O3}$, $(3.6 \pm 0.8) \times 10^{-13}$ cm^3 $molecule^{-1}$ s^{-1}, supports the most recent computational study by Vereecken *et al.*,[22] which reported a rate coefficient of 4×10^{-13} cm^3 $molecule^{-1}$ s^{-1} and a mechanism proceeding via a submerged transition state and chain

addition through bond formation between the negatively charged O atom in O_3 and the positively charged CH_2 group in CH_2OO.

However, the rate coefficients for $CH_2OO + O_3$ and $CH_2OO + IO$ determined in this work are in disagreement with those reported by Chang *et al*.[18] In the previous work, the rate coefficient for $CH_2OO + O_3$ was reported to be $(6.7 \pm 0.5) \times 10^{-14}$ cm^3 molecule^{-1} s^{-1} on the basis of CH_2OO measurements made using time-resolved infrared absorption spectroscopy with O_3 concentrations on the order of 10^{15}–10^{16} molecule cm^{-3}. Although Chang *et al*. were unable to measure IO, the significance of $CH_2OO + IO$ was noted and a combination of numerical simulations and inspection of the intercept of the bimolecular plots (the pseudo-first order rate coefficient describing the loss of CH_2OO as a function of $[O_3]$) was used to estimate a value for $k_{CH2OO+IO}$ of 1.5×10^{-10} cm^3 molecule^{-1} s^{-1} for use in analysis to determine $k_{CH2OO+O3}$. For the UV absorption experiments presented in this work, the rate coefficient for $CH_2OO + IO$ has been determined directly by fitting to the observed CH_2OO concentrations whilst constraining to the model to the observations of IO. In order to investigate the sensitivity of $k_{CH2OO+O3}$ to $k_{CH2OO+IO}$, we performed a series of numerical simulations, using the chemistry system shown in Table 1, in which $k_{CH2OO+IO}$ was fixed to values ranging from zero to 2.0×10^{-10} cm^3 molecule^{-1} s^{-1}, with $k_{CH2OO+I}$ fixed to the value of 1.50×10^{-11} cm^3 molecule^{-1} s^{-1} determined in this work and $k_{CH2OO+O3}$ determined in the fit. Figure 3 shows the variation in $k_{CH2OO+O3}$ and Chi squared (χ^2), which represents the fit quality, with the values for $k_{CH2OO+IO}$ adopted in the model. The minimum in χ^2, indicating the optimum fit result, was obtained for $k_{CH2OO+IO}$ ~8.0×10^{-11} cm^3 molecule^{-1} s^{-1} and gave $k_{CH2OO+O3} = (3.6 \pm 0.8) \times 10^{-13}$ cm^3 molecule^{-1} s^{-1}. Any increase or decrease in $k_{CH2OO+IO}$ relative to the optimum value of ~ 8.0×10^{-11} cm^3 molecule^{-1} s^{-1} resulted in a reduction in the quality of the fit, as indicated by an increase in χ^2.

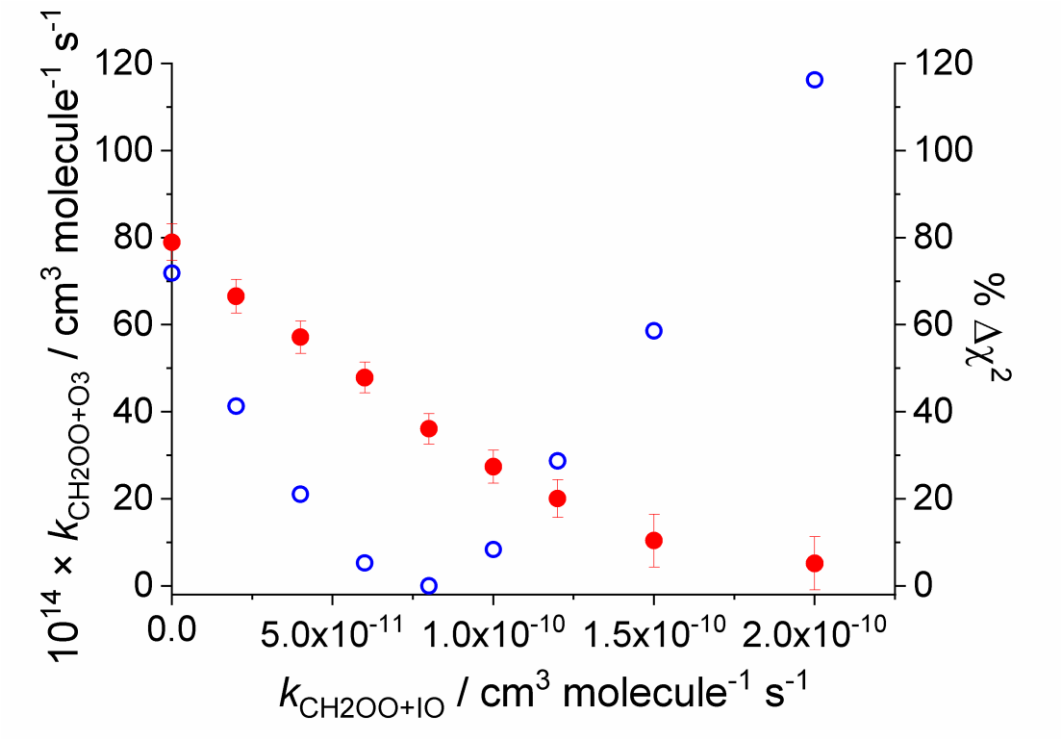

Figure 3: Rate coefficient of the $CH_2OO + O_3$ reaction, $k_{CH2OO+O3}$, (red circles) and percentage change in Chi squared, % $\Delta \chi^2$, (blue circles) for the fit to the data obtained by numerical simulations using values of $k_{CH2OO+IO}$ in the range from (0–2.0) × 10^{-10} cm^3 molecule^{-1} s^{-1}. % $\Delta\chi^2$ was calculated relative to the χ^2 for $k_{CH2OO+IO}$ = 8.0 × 10^{-11} cm^3 molecule^{-1} s^{-1}, where $k_{CH2OO+O3}$ = (3.6 ± 0.8) × 10^{-13} cm^3 molecule^{-1} s^{-1}; uncertainties at 2σ level. During all the numerical simulations $k_{CH2OO+I}$ was fixed to 1.5 × 10^{-11} cm^3 molecule^{-1} s^{-1}.

Using the estimation of $k_{CH2OO+IO}$ = 1.50 × 10^{-10} cm^3 molecule^{-1} s^{-1} adopted by Chang *et al.*, $k_{CH2OO+O3}$ was determined to be (1.0 ± 0.6) × 10^{-13} cm^3 molecule^{-1} s^{-1}, which has overlapping error limits with the value of (6.7 ± 0.5) × 10^{-14} cm^3 molecule^{-1} s^{-1} obtained by Chang *et al.*[18] Figure 4 shows an example fit to CH_2OO observed in this work using a fixed value of $k_{CH2OO+IO}$ = 1.50 × 10^{-10} cm^3 molecule^{-1} s^{-1} in the model. The value of χ^2 when using $k_{CH2OO+IO}$ = 1.50 × 10^{-10} cm^3 molecule^{-1} s^{-1} was ~ 60 % larger than χ^2 when using $k_{CH2OO+IO}$ = 8.0 × 10^{-11} cm^3 molecule^{-1} s^{-1}. In addition, the value of 1.50 × 10^{-10} cm^3 molecule^{-1} s^{-1} is outside the error margins (2σ level) of our result of (7.6 ± 1.4) × 10^{-11} cm^3 molecule^{-1} s^{-1} which was obtained by floating $k_{CH2OO+IO}$ during the numerical simulations. Thus the result shows that an overestimation of $k_{CH2OO+IO}$ leads to an underestimation of the $k_{CH2OO+O3}$.

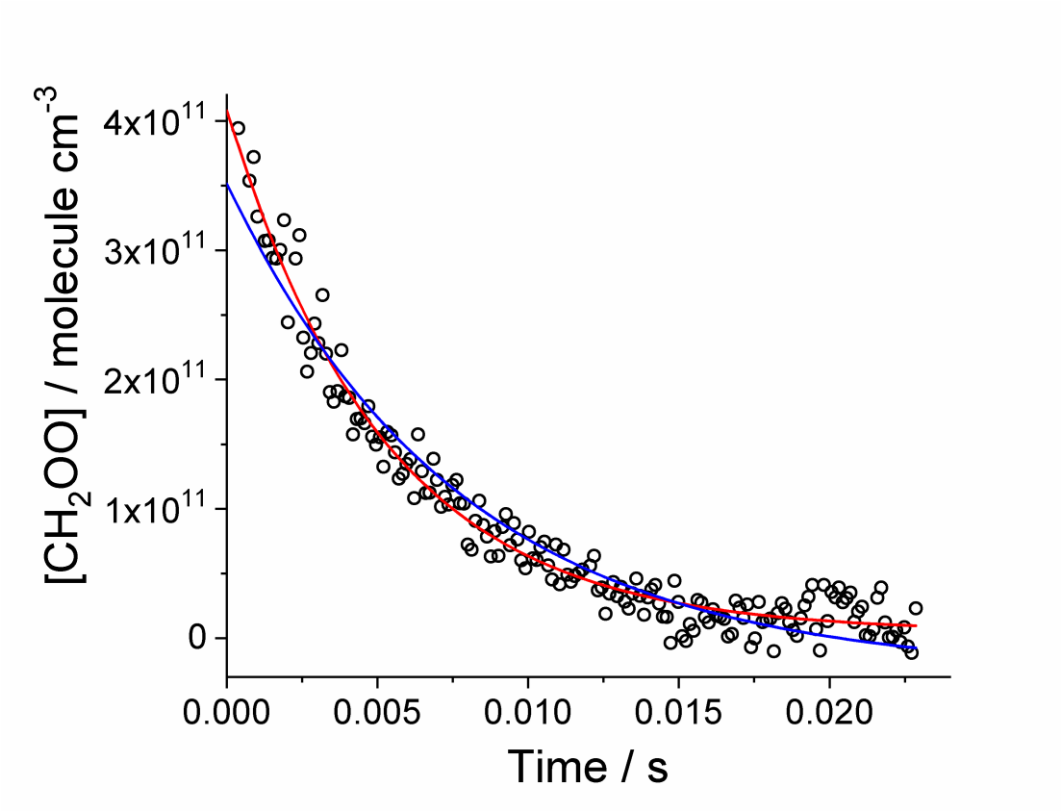

Figure 4: An example of the observations of CH_2OO (black circles) and fit results obtained by numerical integration using the chemistry system described in Table 1 with: $k_{CH2OO+IO} = 8.0 \times 10^{-11}$ cm^3 molecule^{-1} s^{-1} (red line) and $k_{CH2OO+IO} = 1.5 \times 10^{-10}$ cm^3 molecule^{-1} s^{-1} (blue line).

The possibility of particle formation during the kinetic measurements resulting from the use of relatively high [O_3] (~ 10^{15}–10^{16} molecule cm^{-3}) and [CH_2I_2] (~ 0.3–2.0 × 10^{14} molecule cm^{-3}) was also not investigated by Chang *et al.*[18] The formation of iodine oxide (I_xO_y) particles following the UV photolysis (~300–400 nm) of CH_2I_2/O_3 mixtures in the gas phase has been reported previously,[32, 33] and in the present work we found evidence of aerosol formation when [O_3] is in the range ~ 0.5–5.0 × 10^{15} molecule cm^{-3} and [CH_2I_2] is high (~ (1.0–5.0) × 10^{13} molecule cm^{-3}) (see Supporting Information for further details). The results reported previously[18] may therefore have been impacted by the formation of aerosols. The results reported here were obtained in the absence of aerosols as, in contrast with infrared absorption measurements, UV absorption measurements are sensitive to the presence of particles that impact the shape of the measured absorption spectrum (see Supporting Information for further information). The UV absorption measurements thus enable selection of reagent concentrations which avoid any aerosol formation.

Implications for Atmospheric Modelling and Chamber Studies

The rate coefficient measured in this work indicates that the reaction between CH_2OO and O_3 is more than five times faster than suggested by the previous experimental study.[18] For a typical tropospheric O_3 concentration of ~10^{12} molecule cm^{-3}, the rate coefficient determined in this work gives a pseudo-first-order rate coefficient of 0.36 s^{-1} for the loss of CH_2OO via reaction with O_3, which is insufficient to compete with atmospheric losses owing to reactions with water dimers[7] or SO_2.[9, 10] However, ozonolysis experiments in atmospheric simulation chambers are often performed with O_3 concentrations on the order of ~10^{14} molecule cm^{-3},[2, 34, 35] and reactions between SCIs and O_3 are potentially significant under such conditions.[35] The reactions of SCIs with O_3 will significantly affect the total loss rates of SCIs in ozonolysis experiments, and knowledge of the kinetics of such reactions thus have important consequences for our understanding of SCI concentrations in atmospheric simulation chambers. Assuming steady state conditions, and that reaction with O_3 is the sole SCI loss in an alkene ozonolysis experiment, the SCI concentration scales inversely with the rate coefficient for SCI + O_3 and can be estimated from $[SCI]_{SS} = Y_{SCI}\, k_{alkene+O3}[alkene]/k_{SCI+O3}$, where Y_{SCI} is the SCI yield. Table 2 shows the expected steady state concentrations of CH_2OO in investigations of isoprene ozonolysis, assuming an isoprene concentration of 10^{14} molecule cm^{-3} and $Y_{SCI} = 0.28$,[36] for the range of $k_{CH2OO+O3}$ reported in the literature. Knowledge of $k_{CH2OO+O3}$ is thus significant for the understanding and interpretation of CH_2OO concentrations in ozonolysis experiments, and reactions of SCIs with O_3 should be considered in the analysis of such experiments to determine the kinetics and mechanisms of complex atmospheric reactions.

$k_{CH2OO+O3}$ / cm^3 molecule^{-1} s^{-1}	$[CH_2OO]_{SS}$ / molecule cm^{-3}	Reference
$(3.6 \pm 0.8) \times 10^{-13}$	9.9×10^6	This work
$(6.7 \pm 0.5) \times 10^{-14}$	5.3×10^7	Chang *et al.*[18]
4×10^{-13}	8.9×10^6	Vereecken *et al.*[22]
1×10^{-12}	3.6×10^6	Vereecken *et al.*[17]
$< 10^{-20}$	$> 3.6 \times 10^{14}$	Wei *et al.*[20a]
$> 10^{-18}$	$< 3.6 \times 10^{12}$	Kjaergaard *et al.*[19]

Table 2: Steady state concentrations of CH_2OO calculated using $[CH_2OO]_{SS} = Y_{CH2OO}\, k_{C5H8+O3}[C_5H_8]/k_{CH2OO+O3}$, using $k_{C5H8+O3} = 1.27 \times 10^{-17}$ cm^3 molecule^{-1} s^{-1} and $Y_{CH2OO} = 0.28$, as currently adopted in the Master Chemical Mechanism (MCM) for $T = 298$ K,[36] and assuming CH_2OO + O_3 is the only loss reaction for CH_2OO. [a] The rate coefficient given

for the barrier of 14.1 kcal mol^{-1} reported by Wei *et al.*[20] for the reaction between CH_2OO and O_3 was estimated by Vereecken *et al.*[22]

Conclusions

The kinetics of the reactions of the CH_2OO stabilised Criegee intermediate with O_3 and IO have been investigated at 296 K and 300 Torr using simultaneous measurements of CH_2OO and IO made by laser flash photolysis of $CH_2I_2/O_2/O_3$ gas mixtures coupled to time-resolved broadband UV absorption spectroscopy under pseudo-first-order conditions with respect to O_3. Rate coefficients $k_{CH2OO+O3} = (3.6 \pm 0.8) \times 10^{-13}$ cm^3 molecule^{-1} s^{-1} and $k_{CH2OO+IO} = (7.6 \pm 1.4) \times 10^{-11}$ cm^3 molecule^{-1} s^{-1} have been determined in this work, with analysis indicating that the previous measurement of $k_{CH2OO+O3}$ reported in the literature[18] was likely underestimated owing to overestimation of $k_{CH2OO+IO}$.

Challenges associated with theoretical studies of Criegee intermediate chemistry have led to significant discrepancies in predictions of both the mechanism and kinetics of $CH_2OO + O_3$, with predictions of $k_{CH2OO+O3}$ varying from < 10^{-20} to 10^{-12} cm^3 molecule^{-1} s^{-1}.[17, 19, 20, 22] The present study supports the results of the computational study performed by Vereecken *et al.*[22] and provides a much needed point of reference for theoretical determinations of Criegee intermediate reactions.

The reaction between CH_2OO and O_3 is expected to be slow under ambient conditions, but is potentially important in laboratory studies and knowledge of $k_{CH2OO+O3}$ has important consequences for our understanding and interpretation of CH_2OO concentrations in ozonolysis reactions in atmospheric simulation chambers.

Supporting Information

This material is available free of charge *via* the Internet at http://pubs.acs.org.

Author Information

Corresponding Author

Daniel Stone, d.stone@leeds.ac.uk, +44 113 343 6508

Notes

The authors declare no competing financial interest.

Acknowledgements

The authors would like to thank the Natural Environment Research Council (NERC) for funding (grant references NE/L010798/1 and NE/P012876/1). LO thanks Diogo J. Medeiros for help with implementing the model in MATLAB.

References

1. Criegee, R.; Wenner, G. Die Ozonisierung des 9,10-Oktalins. *Ann. Chem. Jus. Liebig* **1949,** *564*, 9-15.

2. Johnson, D.; Marston, G. The Gas-Phase Ozonolysis of Unsaturated Volatile Organic Compounds in the Troposphere. *Chem. Soc. Rev.* **2008,** *37*, 699-716.

3. Nguyen, T. B.; Tyndall, G. S.; Crounse, J. D.; Teng, A. P.; Bates, K. H.; Schwantes, R. H.; Coggon, M. M.; Zhang, L.; Feiner, P.; Milller, D. O., et al. Atmospheric Fates of Criegee Intermediates in the Ozonolysis of Isoprene. *Phys. Chem. Chem. Phys.* **2016,** *18*, 10241-10254.

4. Heard, D. E.; Carpenter, L. J.; Creasey, D. J.; Hopkins, J. R.; Lee, J. D.; Lewis, A. C.; Pilling, M. J.; Seakins, P. W.; Carslaw, N.; Emmerson, K. M. High Levels of the Hydroxyl Radical in the Winter Urban Troposphere. *Geophys. Res. Lett.* **2004,** *31*, 1-5.

5. Harrison, R. M.; Yin, J.; Tilling, R. M.; Cai, X.; Seakins, P. W.; Hopkins, J. R.; Lansley, D. L.; Lewis, A. C.; Hunter, M. C.; Heard, D. E., et al. Measurement and Modelling of Air Pollution and Atmospheric Chemistry in the UK West Midlands Conurbation: Overview of the PUMA Consortium Project. *Sci. Tot. Env.* **2006,** *360*, 5-25.

6. Berndt, T.; Kaethner, R.; Voigtlander, J.; Stratmann, F.; Pfeifle, M.; Reichle, P.; Sipila, M.; Kulmala, M.; Olzmann, M. Kinetics of the Unimolecular Reaction of CH_2OO and the Bimolecular Reactions with the Water Monomer, Acetaldehyde and Acetone Under Atmospheric Conditions. *Phys. Chem. Chem. Phys.* **2015,** *17*, 19862-19873.

7. Lewis, T. R.; Blitz, M. A.; Heard, D. E.; Seakins, P. W. Direct Evidence for a Substantive Reaction Between the Criegee Intermediate, CH_2OO, and the Water Vapour Dimer. *Phys. Chem. Chem. Phys.* **2015,** *17*, 4859-4863.

8. Sheps, L.; Rotavera, B.; Eskola, A. J.; Osborn, D. L.; Taatjes, C. A.; Au, K.; Shallcross, D. E.; Khan, M. A. H.; Percival, C. J. The Reaction of Criegee Intermediate CH_2OO with Water Dimer: Primary Products and Atmospheric Impact. *Phys. Chem. Chem. Phys.* **2017,** *19*, 21970-21979.

9. Welz, O.; Savee, J. D.; Osborn, D. L.; Vasu, S. S.; Percival, C. J.; Shallcross, D. E.; Taatjes, C. A. Direct Kinetic Measurements of Criegee Intermediate (CH_2OO) Formed by Reaction of CH_2I with O_2. *Science* **2012,** *335*, 204-207.

10. Stone, D.; Blitz, M.; Daubney, L.; Howes, N. U. M.; Seakins, P. Kinetics of CH_2OO Reactions with SO_2, NO_2, NO, H_2O and CH_3CHO as a Function of Pressure. *Phys. Chem. Chem. Phys.* **2014,** *16*, 1139-1149.

11. Howes, N. U. M.; Mir, Z. S.; Blitz, M. A.; Hardman, S.; Lewis, T. R.; Stone, D.; Seakins, P. W. Kinetic Studies of C_1 and C_2 Criegee Intermediates with SO_2 using Laser Flash Photolysis

Coupled with Photoionization Mass Spectrometry and Time Resolved UV Absorption Spectroscopy. *Phys. Chem. Chem. Phys.* **2018,** *20*, 22218-22227.

12. Chhantyal-Pun, R.; Davey, A.; Shallcross, D. E.; Percival, C. J.; Orr-Ewing, A. J. A Kinetic Study of the CH_2OO Criegee Intermediate Self-Reaction, Reaction with SO_2 and Unimolecular Reaction using Cavity Ring-Down Spectroscopy. *Phys. Chem. Chem. Phys.* **2015,** *17*, 3617-3626.

13. Caravan, R. L.; Khan, M. A. H.; Rotavera, B.; Papajak, E.; Antonov, I. O.; Chen, M. W.; Au, K.; Chao, W.; Osborn, D. L.; Lin, J. J. M., et al. Products of Criegee Intermediate Reactions with NO_2: Experimental Measurements and Tropospheric Implications. *Farad. Discuss.* **2017,** *200*, 313-330.

14. Mir, Z. S.; Lewis, T.R.; Onel, L.; Blitz, M.A.; Seakins, P.W.; Stone, D. CH_2OO Criegee Intermediate UV Absorption Cross-Sections and Kinetics of CH_2OO + CH_2OO and CH_2OO + I as a Function of Pressure. *Phys. Chem. Chem. Phys.* **2020,** *22*, 9448-9459.

15. Buras, Z. J.; Elsamra, R. M. I.; Jalan, A.; Middaugh, J. E.; Green, W. H. Direct Kinetic Measurements of Reactions between the Simplest Criegee Intermediate CH_2OO and Alkenes. *J. Phys. Chem. A* **2014,** *118*, 1997-2006.

16. Decker, Z. C. J.; Au, K.; Vereecken, L.; Sheps, L. Direct Experimental Probing and Theoretical Analysis of the Reaction Between the Simplest Criegee Intermediate CH_2OO and Isoprene. *Phys. Chem. Chem. Phys.* **2017,** *19*, 8541-8551.

17. Vereecken, L.; Harder, H.; Novelli, A. The Reactions of Criegee Intermediates with Alkenes, Ozone, and Carbonyl Oxides. *Phys. Chem. Chem. Phys.* **2014,** *16*, 4039-4049.

18. Chang, Y.-P.; Chang, H.-H.; Lin, J. J.-M. Kinetics of the Simplest Criegee Intermediate Reaction with Ozone Studied Using a Mid-Infrared Quantum Cascade Laser Spectrometer. *Phys. Chem. Chem. Phys.* **2018,** *20*, 97-102.

19. Kjaergaard, H. G.; Kurten, T.; Nielsen, L. B.; Jorgensen, S.; Wennberg, P. O. Criegee Intermediates React with Ozone. *J. Phys. Chem. Lett.* **2013,** *4*, 2525-2529.

20. Wei, W. M.; Zheng, R. H.; Pan, Y. L.; Wu, Y. K.; Yang, F.; Hong, S. Ozone Dissociation to Oxygen Affected by Criegee Intermediate. *J. Phys. Chem. A* **2014,** *118*, 1644-1650.

21. Maranzana, A.; Tonachini, G. Multireference Study of the H_2COO (Criegee Intermediate) + O_3 Addition: A Reaction of Possible Tropospheric Interest. *J. Phys. Chem. A* **2020,** *124*, 1112-1120.

22. Vereecken, L.; Rickard, A. R.; Newland, M. J.; Bloss, W. J. Theoretical Study of the Reactions of Criegee Intermediates with Ozone, Alkylhydroperoxides, and Carbon Monoxide. *Phys. Chem. Chem. Phys.* **2015,** *17*, 23847-23858.

23. Stone, D.; Au, K.; Sime, S.; Medeiros, D. J.; Blitz, M.; Seakins, P. W.; Decker, Z.; Sheps, L. Unimolecular Decomposition Kinetics of the Stabilised Criegee Intermediates CH_2OO and CD_2OO. *Phys. Chem. Chem. Phys.* **2018,** *20*, 24940-24954.

24. Lewis, T.; Heard, D. E.; Blitz, M. A. A Novel Multiplex Absorption Spectrometer for Time-Resolved Studies. *Rev. Sci. Instr.* **2018,** *89,* 1-9.

25. Burkholder, J. B.; Sander, S. P.; Abbatt, J. P. D.; Barker, J. R.; Huie, R. E.; Kolb, C. E.; Kurylo, M. J.; Orkin, V. L.; Wilmouth, D. M.; Wine, P. H. Chemical Kinetics and Photochemical Data for Use in Atmospheric Studies - Evaluation No. 18. JPL Publication 15-10. **2015**, http://jpldataeval.jpl.nasa.gov/, (accessed 15 April 2020).

26. Spietz, P.; Gomez Martin, J. C.; Burrows, J. P. Spectroscopic Studies of the I_2/O_3 Photochemistry. Part 2. Improved Spectra of Iodine Oxides and Analysis of the IO Absorption Spectrum. *J. Photochem. Photobiol. A: Chem.* **2005,** *176*, 50-67.

27. Ting, W. L.; Chang, C. H.; Lee, Y. F.; Matsui, H.; Lee, Y. P.; Lin, J. J. M. Detailed Mechanism of the $CH_2I + O_2$ Reaction: Yield and Self-Reaction of the Simplest Criegee Intermediate CH_2OO. *J. Chem. Phys.* **2014,** *141,* 1-11.

28. Foreman, E. S.; Murray, C. Kinetics of IO Production in the $CH_2l + O_2$ Reaction Studied by Cavity Ring-Down Spectroscopy. *J. Phys. Chem. A* **2015,** *119*, 8981-8990.

29. Gravestock, T. J.; Blitz, M. A.; Bloss, W. J.; Heard, D. E. A Multidimensional Study of the Reaction $CH_2I + O_2$: Products and Atmospheric Implications. *Chem. Phys. Chem.* **2010,** *11*, 3928-3941.

30. Tucceri, M. E.; Dillon, T. J.; Crowley, J. N. A Laser Photolysis-Resonance Fluorescence Study of the Reactions: $I + O_3 \rightarrow IO + O_2$, $O + I_2 \rightarrow IO + I$, and $I + NO_2 + M \rightarrow INO_2 + M$ at 298 K. *Phys. Chem. Chem. Phys.* **2005,** *7*, 1657-1663.

31. Jenkin, M. E.; Cox, R. A.; Mellouki, A.; Lebras, G.; Poulet, G. Kinetics of the Reaction of Iodine Atoms with HO_2 Radicals. *J. Phys. Chem.* **1990,** *94*, 2927-2934.

32. Hoffmann, T.; O'Dowd, C. D.; Seinfeld, J. H. Iodine Oxide Homogeneous Nucleation: An Explanation for Coastal New Particle Production. *Geophys. Res. Lett.* **2001,** *28*, 1949-1952.

33. Jimenez, J. L.; Bahreini, R.; Cocker, D. R.; Zhuang, H.; Varutbangkul, V.; Flagan, R. C.; Seinfeld, J. H.; O'Dowd, C. D.; Hoffmann, T. New Particle Formation from Photooxidation of Diiodomethane (CH_2I_2). *J. Geophys. Res. - Atmos.* **2003,** *108*, 1-25.

34. Malkin, T. L.; Goddard, A.; Heard, D. E.; Seakins, P. W. Measurements of OH and HO_2 Yields from the Gas Phase Ozonolysis of Isoprene. *Atmos. Chem. Phys.* **2010,** *10*, 1441-1459.

35. Novelli, A.; Vereecken, L.; Lelieveld, J.; Harder, H. Direct Observation of OH Formation from Stabilised Criegee Intermediates. *Phys. Chem. Chem. Phys.* **2014,** *16*, 19941-19951.

36. Saunders, S. M.; Jenkin, M. E.; Derwent, R. G.; Pilling, M. J. Protocol for the Development of the Master Chemical Mechanism, MCM v3 (Part A): Tropospheric Degradation of Non-Aromatic Volatile Organic Compounds. *Atmos. Chem. Phys.* **2003,** *3*, 161-180.

TOC Image